

Article

Hydrothermal Carbonization of the Wet Fraction from Mixed Municipal Solid Waste: A Fuel and Structural Analysis of Hydrochars

Maciej Śliz ^{1,*}, Klaudia Czerwińska ¹, Aneta Magdziarz ¹, Lidia Lombardi ² and Małgorzata Wilk ¹

¹ Department of Heat Engineering and Environment Protection, AGH University of Science and Technology, Mickiewicza 30 Av., 30-059 Krakow, Poland

² Niccolò Cusano University, Via Don Carlo Gnocchi 3, 00166 Rome, Italy

* Correspondence: msliz@agh.edu.pl

Abstract: One of the by-products of a mechanical-biological waste treatment plant is the under-sieve fraction, which requires separation prior to further processing of municipal mixed waste. This stream usually follows the fate of landfilling. Instead, it could be introduced to the hydrothermal carbonization (HTC) process to improve its fuel properties and become solid recovered fuel. The organic fraction and high moisture content (approximately 26%) of under-sieve fraction are favorable properties for the HTC process. In this study, hydrochars, the solid product of HTC, were produced at 200 and 220 °C with residence times of 1, 4, and 8 h. The main aim of this investigation was to establish the influence of different process parameters on hydrochars' fuel properties. Thermogravimetric analysis (TGA), Fourier-transform infrared spectroscopy (FTIR), and scanning electron microscopy (SEM) were employed in the analyses. The results confirmed the positive effects of hydrothermal carbonization on the under-sieve fraction of municipal mixed waste properties. The ignition temperature increased from 247 °C to 288 °C and burnout temperature decreased to 443 °C from 489 °C after hydrothermal carbonization, causing a shorter combustion process. The determined key combustion parameters were: $S = 12.4 \times 10^{-8} \text{ min}^{-2} \cdot \text{C}^{-3}$, $H_f = 1174.9 \text{ °C}$ and $Di = 0.0075\% \cdot \text{min}^{-3}$, which in comparison to USF decreased by 44%, increased by 33%, and decreased by 29%, respectively, and became closer to those of coal. Furthermore, the identified structural changes indicate that hydrochars could be successfully used in energy production. The most promising results were found for hydrochar produced at 220 °C for 1 h, leading to a better combustion performance and providing a more stable and a less violent flame.

Keywords: hydrothermal carbonization; municipal solid waste; TGA; FTIR; SEM-EDS



Citation: Śliz, M.; Czerwińska, K.; Magdziarz, A.; Lombardi, L.; Wilk, M. Hydrothermal Carbonization of the Wet Fraction from Mixed Municipal Solid Waste: A Fuel and Structural Analysis of Hydrochars. *Energies* **2022**, *15*, 6708. <https://doi.org/10.3390/en15186708>

Academic Editor: Attilio Converti

Received: 17 August 2022

Accepted: 8 September 2022

Published: 14 September 2022

Publisher's Note: MDPI stays neutral with regard to jurisdictional claims in published maps and institutional affiliations.



Copyright: © 2022 by the authors. Licensee MDPI, Basel, Switzerland. This article is an open access article distributed under the terms and conditions of the Creative Commons Attribution (CC BY) license (<https://creativecommons.org/licenses/by/4.0/>).

1. Introduction

Recently, hydrothermal carbonization has more often been brought to attention as a process that can change and improve the properties of various feedstock. Due to the reactions achieved in an aqueous environment, it is a suitable treatment for wet materials with unfavorable, high organic content, e.g., vegetation, food and paper waste, sewage sludge, or mixed solid waste [1–9]. Generally, the latter, municipal mixed waste, is treated in a mechanical-biological treatment plant where the recycling of metal from waste is processed and then the remaining residue is aerobically stabilized and landfilled. However, according to European legislation, the quantity of waste that is landfilled must decrease to a limit of 10% by 2035, hence, other solutions are being sought [10]. Accordingly, hydrothermal carbonization is suggested as a suitable method to improve dewatering, grinding, handling, transportation, and storage of the wet feedstock. Moreover, the elevated temperature and pressure guarantee an altered structure of the material as well as limiting the biodegradation process. Furthermore, the reactions that occur during hydrothermal

treatment, e.g., hydrolysis, dehydration, decarboxylation, polymerization and aromatization, provide lower oxygen and higher carbon content in the final product [11]. Those properties, supported by an increased calorific value, create an environmentally-friendly solid recovered fuel, hydrochar, which could be successfully applied to energy systems, e.g., in an incineration plant. Additionally, the hydrothermal treatment of post-processing organic waste is in concordance with the waste-to-energy and minimizing of waste at source European environmental policy [12].

Consequently, the hydrothermal carbonization process is often studied to establish the possible application of hydrochars and to find the best process parameters for the process, which could minimize costs and maximize possible benefits [13,14]. For instance, Santos et al. [15] studied hydrochars derived from the hydrothermal carbonization process of low-grade organic fraction of municipal solid waste (OFMSW) at 180 °C for 2 h as a novel, sustainable, low-CO₂ building material for thermal insulation panels. In addition, Ischia [16] studied this material under similarly mild conditions (180 °C) but applied thermal and chemical extraction (1:4 methanol: dichloromethane) on hydrochars. The removal of reactive volatile matter in hydrochars was investigated during thermal treatment and chemical extraction, suggesting a potential pathway for the recovery of fatty acids and condensation of fuel molecules in the solid hydrochar. Furthermore, the relevant properties of hydrochar could be used as a soil amendment or an environmental adsorbent as well as simultaneously extracting valuable biodiesel and biofuel precursors [16]. Aragon-Briceno et al. [17] studied the optimum hydrothermal carbonization process conditions for recovering water from the MSW digestate at three temperatures 180, 200, and 230 °C and three residence times 30, 60, and 120 min and proved that the most suitable conditions were 200 °C with a residence time of 120 min, resulting in 47.2% of water recovery. Based on the net energy balance (5.6 MJ) and the applied Aspen model, the integration of HTC as part of the dewatering system of an MSW treatment plant was proposed and provided very promising results. Espro et al. [18] investigated hydrochars derived from orange peels in sensing applications. Hydrochars produced at 300 °C were used to fabricate high performance conductometric sensors for the monitoring of NO₂.

Furthermore, Roman et al. [19] studied different residence times (1–5 h), on a quantity of compost derived from MSW (1–4 g in 30 mL) and at different temperatures (150–230 °C) regarding the mass and energy yield of hydrochars and, most importantly, on post-processing water disposal, while searching for the catalytic behavior of both products. On the contrary, Lin et al. [20] studied the behavior of four typical components of municipal solid waste (MSW), such as waste textile, wood, paper, and food under hydrothermal and co-hydrothermal carbonization. The blends of MSW and waste textile derived at 240 °C and 90 min with a 1:12 solid/liquid ratio exhibited synergistic effects during the co-HTC of typical MSW components. The co- and hydrochars behavior and characteristics' parameters of combustion were studied by profound analysis of TG and DTG data. Moreover, it was found that hydrochars more stably combusted and effectively fitted the nth-order kinetic model of the combustion reaction process. Venna et al. [21] also confirmed the potential of hydrochar derived from municipal solid waste, namely yard and food waste, as a solid biofuel. In comparison to distilled water, a landfill leachate was applied as a water carrier in the HTC process, but fuel characteristics of the hydrochars did not significantly change. TGA was implemented to describe the combustion behavior and parameters of the derived hydrochars. Moreover, the morphology and surface chemistry of the hydrochars was applied to detect the morphological changes caused by the HTC process. SEM images depicted microspheres, higher porosity, and surface roughness after hydrothermal degradation resulted in better fuel characteristics. The changes in functional groups in hydrochar in comparison to raw samples were determined by FTIR examination. These techniques were also used by Wang et al. [22] to study food waste and their hydrochars produced within a temperature range of 180–260 and 60 min of residence time in terms of solid biofuels characteristics. Akarsu et al. [23], Saqib et al. [24], and Nguyen et al. [25] also studied food waste and their hydrochars to confirm their ability in energy production by emphasizing

their physicochemical, structural, and combustion performance. Sharma et al. [26] studied in detail the mechanism and process parameters of the hydrothermal carbonization of municipal solid waste as a potential biofuel taking into account the environmental impact. It was suggested that the optimized parameters of the process can ensure the improved properties of hydrochars identified by advanced instrumental methods for a net renewable energy production potential value.

The need for a profound discussion concerning the hydrothermal carbonization of municipal solid waste in order to fully understand its behavior was underlined by many researchers [5,27–31]. Accordingly, in this study, the hydrothermal carbonization of municipal solid waste is investigated in detail, in particular under-sieve mixed waste, mainly focused on the fuel properties of hydrochar derived under various conditions of the process.

2. Materials and Methods

The stream of municipal mixed waste, investigated in this research, was collected from a rotating sieve drum at an Italian mechanical-biological treatment plant. The particles of material were smaller than 60 mm and referred to as under-sieve fraction (USF)—Figure 1. The USF was grey, fluffy, and resembled dust. A composition analysis of USF identified some paper, plastics, glass, wood, textiles, food waste, coffee pods, inert materials, and metals [32]. However, approximately 75% of the USF proved to be indistinguishable due to its small size—Figure 2. To simplify handling of the samples the material was dried and milled.



Figure 1. Under-sieve fraction of municipal mixed waste prior to and after hydrothermal carbonization.

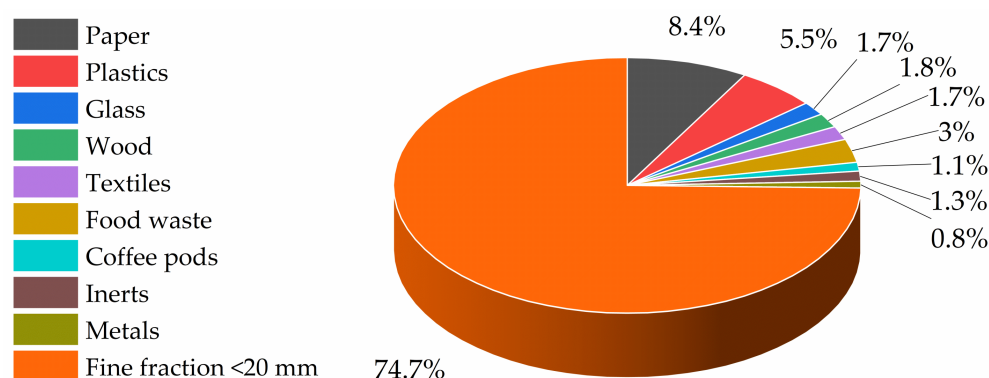


Figure 2. Composition of under-sieve fraction of municipal mixed waste [32].

For hydrothermal carbonization, a 1000 mL, stainless steel, Zipperclave® Stirred Reactor (Parker Autoclave Engineers, Erie, PA, USA) was used. The schematic of the experimental set-up is presented in Figure 3. The USF was mixed with deionized water prior to the experiment, achieving 0.15 dry solids to water ratio. The experiments were

conducted at 200 and 220 °C with reaction times of 1, 4, and 8 h measured from the moment the reactor was heated to the desired temperature. During the process, the mixture was constantly stirred and afterwards immediately cooled down by feeding cold water through the coil inside the reactor. The separation of solid and liquid products was conducted via vacuum filtration. The produced hydrochars were dried at 105 °C in an oven overnight and stored in sealed containers prior to further analyses. The hydrochars were brown in color and with an increase in the process temperature or residence time the color became darker. After hydrothermal carbonization the material can be easily ground after drying. Additional information about the USF and hydrochars can be found in a previous publication by Śliz et al. [32].

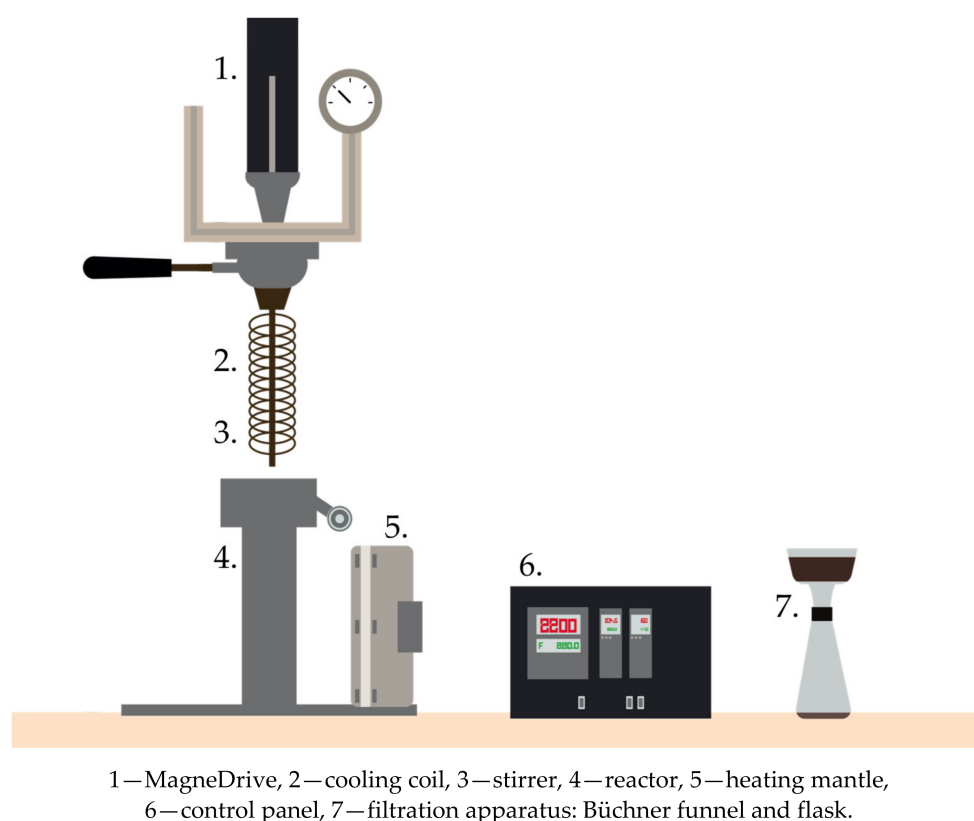


Figure 3. Experimental setup used for hydrothermal carbonization and filtration [32].

The proximate and ultimate analyses were performed by a muffle furnace according to European Standards (EN 15414–3:2011, EN 15403:2011, and EN 15402:2011) and a Truspec LECO 628 CHNS Analyzer (PKN-ISO/TS 12902:2007), respectively. Additionally, the high heating value determination was carried out by means of a LECO AC500 Isoperibol Calorimeter (DIN 51,900 and ISO 1928).

The combustion process was investigated by means of thermal analysis in an air atmosphere. Samples deposited in the crucible were heated from room temperature up to 700 °C at a heating rate of 10 °C/min. This method enables TG, DTG, and DSC curves for USF and hydrochars to be presented.

Moreover, based on those results, the characteristic parameters of the combustion process were determined. Among them an ignition temperature, T_i , and a burnout temperature, T_b , should be distinguished. According to the literature, the ignition temperature (point C) can be found at the intersection of the horizontal line drawn from point B, when devolatilization started, and a tangent line drawn from point A, where the vertical line from the first DTG peak crosses the TG line. The burnout temperature was found at the mass stabilization point where the mass loss rate decreased to below 1%/min [33,34]. Combustibility indices, such as the ignition index (D_i), were also included:

$$D_i = \frac{DTG_1}{t_1 \cdot t_i}$$

where DTG_1 is the value of the highest mass loss rate (first peak in the DTG curve), t_1 and t_i are the times of occurrence of this first peak and when the ignition temperature was reached, respectively. The sooner the ignition started and the highest mass loss rate was achieved, the higher the value of the D_i index reached. This corresponds with an easy release of volatile matter and simple ignition. Next, is the burnout index (D_b):

$$D_b = \frac{DTG_1}{\Delta t_{0.5} \cdot t_1 \cdot t_b}$$

where $\Delta t_{0.5}$ is the time at which the mass loss rate reached half of its maximum value and t_b is the time the combustion process takes to reach burnout temperature. The lower value of D_b required less time to complete the combustion process. The comprehensive combustion index (CCI or S) follows:

$$S = \frac{DTG_1 \cdot DTG_{mean}}{T_i^2 \cdot T_b}$$

where DTG_{mean} is the mean value of the mass loss rate. It reflects the ignition, combustion, and burnout properties of the fuel. Higher values of the S index indicate easy combustion at an early stage [35]. The combustion stability index (CSI or H_f) is calculated according to the following equation:

$$H_f = T_1 \cdot \ln\left(\frac{\Delta t_{0.5}}{DTG_{mean}}\right)$$

where T_1 is the temperature corresponding to DTG_1 . Index H_f expresses the rate and intensity of the combustion process in which lower values are preferred. Combustibility indices were calculated based on equations presented by Mureddu et al. [36,37].

To investigate the morphology of the samples, a scanning electron microscope, (SEM) FEI Inspect S50, was employed and supported by the energy dispersive X-ray spectroscopy (EDS). Fourier-transform infrared spectroscopy was conducted with the Nicolet 6700 FTIR (Thermo Scientific, Waltham, MA, USA), including the attenuated total reflectance module to assess changes in bonds of municipal mixed solid waste.

3. Results and Discussions

To summarize the results of proximate analysis, a Tanner diagram is presented in Figure 4. It has been established that for the combustion of municipal solid waste certain requirements have to be met. Namely, the moisture content cannot exceed 50%, ash content cannot be higher than 60%, and combustible fraction has to be at least 25% [38]. The materials which meet those restrictions are depicted in the bottom right corner of the triangle diagram (grey area). Herein, the hydrochars were dried after the HTC process and easily fulfilled those requirements. However, an increase in the moisture content would cause them to move up and slightly to the left side of the diagram (simultaneously, the ash and combustible fraction content would decrease), which should retain them in the highlighted area of the autothermic combustion. Similar conclusions were presented by Komilis et al. for municipal solid waste [39]. The results of the proximate and ultimate analyses can be found in Table 1. The detailed description, presented in previous publication concerns the under-sieve fraction of municipal mixed solid waste [32]. Nevertheless, to summarize the key changes in the properties of hydrochars, it could be concluded that with a longer residence time and a higher reaction temperature, it would cause a higher value of high heating value and a lower mass yield (ratio of hydrochar mass to feedstock mass). An increase in the ash content with a longer reaction time was also a noticeable trend. The correlation between the process parameters and the analysis results is also in accordance with general trends found by various researchers investigating the hydrothermal carbonization process [7,40].

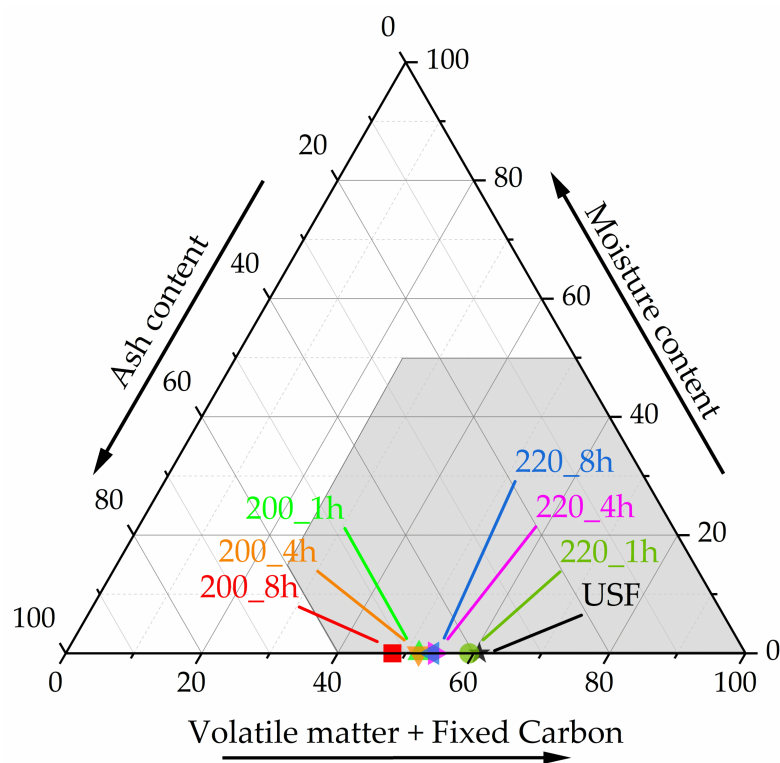


Figure 4. Composition of the under-sieve fraction of municipal mixed waste.

Table 1. Results of ultimate and proximate analysis [32].

	C,%	H,%	N,%	S,%	O,%	A,%	VM,%	FC,%	HHV, MJ/kg
USF	36.0	5.2	1.3	0.2	18.1	39.2	51.7	9.2	14.6
200_1 h	32.6	4.2	0.8	0.5	13.9	48.0	45.9	6.1	13.5
200_4 h	33.7	4.2	0.9	0.5	12.6	48.1	45.0	6.9	14.2
200_8 h	32.3	4.0	1.0	0.5	10.2	52.0	42.7	5.3	14.4
220_1 h	38.3	4.7	0.9	0.1	15.3	40.7	48.4	11.0	16.4
220_4 h	38.2	4.5	1.1	0.2	10.3	45.7	42.0	12.3	16.7
220_8 h	40.5	4.8	1.3	0.3	7.0	46.1	42.9	11.0	18.5

3.1. Thermogravimetric Analysis

The results of the thermogravimetric analysis are presented in Figures 5 and 6. The combustion profiles are depicted in the form of TG and DTG curves. The shape of those curves clearly represents the influence of the reaction time on the combustion performance of hydrochars. A typical combustion process can be divided into three stages [12,41]. The first stage, which starts almost immediately after increasing the temperature to above room temperature and lasts to circa 150 °C, is connected with moisture release. Herein, this stage was omitted as the samples were dried after the separation of the phases following the experiments. The beginning of the next stage is marked by the ignition temperature. In Figure 5, depicted in green, the volatile matter is released and combusted. For USF, the T_i equals 247 °C and at this stage the highest mass drop occurs. The first DTG peaks have a value of 5.973%/min and were found at 289 °C. In the next step, the mass loss rate decreases, and at a higher temperature the last stage concerning the combustion of char is distinguished—marked as stage II and depicted in blue. The second DTG peak is much lower (2.332%/min at 463 °C for USF). The burnout temperature was 489 °C and subsequently the mass loss stabilized. Hydrochars in general, have a higher mass of residue after the combustion process and a lower volatile matter content in comparison to an untreated sample, as a mass loss begins at higher temperatures. After hydrothermal carbonization the first DTG peak becomes lower and switches to higher temperatures

in the range of 325 to 332 °C for all of the hydrochars [42,43]. Based on these results, it could be stated that the HTC process evidently causes the decrease in the combustion time. The ignition temperature rises due to the decrease in the volatile matter content. The samples 200_1 h and 220_1 h presented the highest ignition temperatures, 288 °C and 282 °C, respectively. However, after a longer reaction time of 8 h, the ignition temperatures decreased reaching 273 °C for hydrochar derived at 200 °C and 256 °C for hydrochar treated at 220 °C. Simultaneously, burnout occurs at lower temperatures, 443 °C for samples carbonized at 200 °C and c.a. 463–477 °C for those pretreated at 220 °C. Moreover, the mass rate loss in the first stage of combustion was maintained only for samples treated for 1 h and is close to 6%/min. Samples treated for 4 and 8 h of residence time dipped to 3.8 and 2.7%/min at 200 °C, and to 3.6 and 3.2 at 220 °C.

Furthermore, the temperatures in the second stage of combustion decreased. For USF it was 409 °C, while for samples retained at 200 °C it was closer to 375 °C, and for those treated at 220 °C it was 10 °C higher at 385 °C.

The analysis of TG and DTG profiles not only presents the combustion performance but are also the basis for assessing the key combustion factors summarized in Table 2. Among them combustion indices should be distinguished. A lower ignition index (D_i), which dropped from 0.0106%·min⁻³ for USF to the lowest value of 0.0036%·min⁻³ for sample 220_8 h, corresponds to a lower volatile matter content and a higher ignition temperature. Index S connects the ease of ignition, burning velocity and burnout temperature. The highest value for USF, $22.0 \times 10^{-8}\%$ ·min⁻²·°C⁻³, indicates that it ignites faster and more intensively than in the case of hydrochars—a lower ignition temperature and a high mass loss rate [44]. Conversely, the lowest value, $4.6 \times 10^{-8}\%$ ·min⁻²·°C⁻³, was reached for hydrochar derived at 220_8 h. Similarly, the lowest value of the H_f index for USF suggests better combustion properties [35,36]. A few trends can be noticed when comparing results calculated for hydrochars obtained at different parameters. Prolonging the reaction time from 1 to 8 h causes a decrease in fuel properties estimated by combustibility indices. By comparing the processing temperature, the following observation could be made: when a higher temperature was applied, stronger effects were observed. In addition, it should be noted that the HTC process increased the ignition temperature but a longer residence time caused a decrease in its value, whereas the burnout temperatures were lower for hydrochars than for feedstock. At the same time, the first DTG peak occurred at a higher temperature for hydrochars, approximately 330 °C, than for feedstock, 289 °C. A similar observation on the influence of HTC on the combustion process was presented by Arellano et al. [45]. In summary, hydrothermal carbonization does not significantly improve the fuel properties of the under-sieve fraction of municipal solid waste, but it probably slightly improves the stability of the combustion process due to the release of a lower content of volatile matter.

Table 2. Combustion parameters estimated by means of thermogravimetric analysis.

	T_i °C	t_i min	T_b °C	t_b min	T_1 °C	t_1 min	DTG_1 %/min	$t_{0.5}$ min	DTG_{mean} %/min	D_i %·min ⁻³	D_b %·min ⁻⁴	S %·min ⁻² ·°C ⁻³	H_f °C
USF	247	21.77	489	45.47	289	25.85	5.973	23.08	1.097	0.0106	22.0×10^{-5}	22.0×10^{-8}	880.3
200_1 h	288	26.32	443	41.80	327	30.10	5.934	27.80	1.007	0.0083	18.0×10^{-5}	16.7×10^{-8}	1069.4
200_4 h	276	25.17	443	41.85	329	30.33	3.822	26.85	0.782	0.0053	10.9×10^{-5}	8.7×10^{-8}	1146.2
200_8 h	273	24.85	442	41.72	330	30.45	2.697	26.32	0.945	0.0048	10.6×10^{-5}	9.7×10^{-8}	1057.0
220_1 h	282	25.12	464	42.98	326	29.38	6.099	26.78	0.765	0.0075	17.0×10^{-5}	12.4×10^{-8}	1174.9
220_4 h	265	23.45	463	42.87	325	29.28	3.624	26.58	0.684	0.0050	11.2×10^{-5}	7.8×10^{-8}	1207.3
220_8 h	256	22.60	477	44.32	332	29.87	3.207	22.80	0.565	0.0036	8.1×10^{-5}	4.6×10^{-8}	1267.5

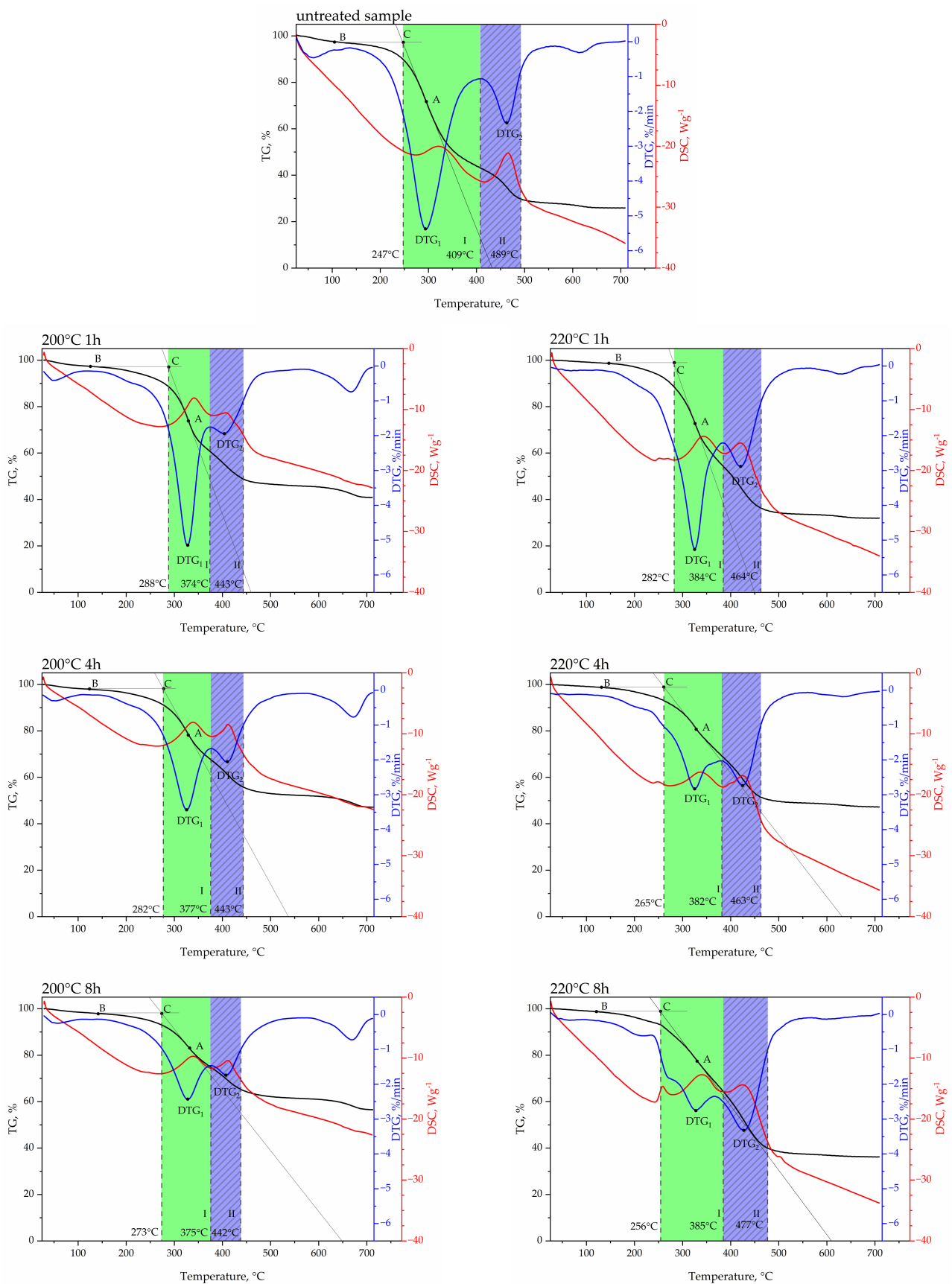


Figure 5. Summary of TG and DTG curves for each experiment conducted at 200 °C and 220 °C for 1, 4, and 8 h.

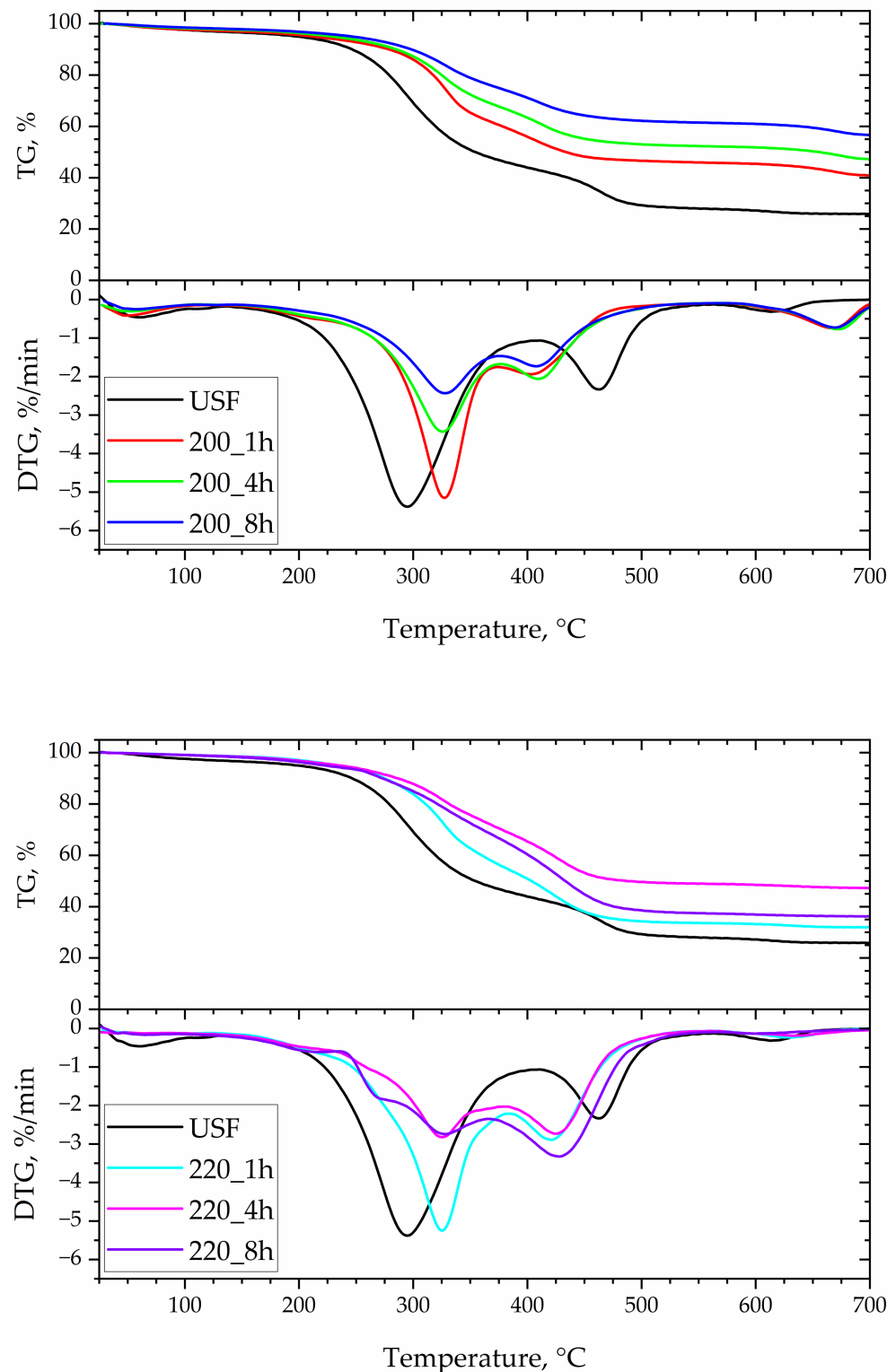


Figure 6. Comparison of TG and DTG curves for samples hydrothermally treated at 200 and 220 °C.

3.2. Fourier-Transform Infrared Spectroscopy

Hydrochars present a similarly shaped curve on the FTIR diagram (Figure 7) as untreated USF. The most important peaks with corresponding bonds are illustrated in Table 3. The increase of the reaction time caused a decrease in the peaks, which became less distinguishable. Nevertheless, a wide mound at approximately $3100\text{--}3600\text{ cm}^{-1}$ that spiked at approximately $3330\text{--}3340\text{ cm}^{-1}$ is identified as a characteristic stretching O–H vibration

in hydroxyl or carboxyl groups. Its decrease with a longer reaction time and higher process temperature indicates that those factors facilitate dehydration [46,47]. Double peaks, in the range of 2860–2930 cm^{-1} represent the stretching vibration of the C–H bond in aromatic and aliphatic compounds. Their presence indicates unsaturation [21,48]. The disappearing peak at 1740 cm^{-1} is associated with the stretching of C=O in alkali esters in hemicellulose. The decreasing signal at approximately 874 cm^{-1} supports degradation of hemicellulose in HTC conditions. Moreover, the peaks at 1516 cm^{-1} and 1454 cm^{-1} are clearly visible for the sample after hydrothermal carbonization and prove the presence of lignin, which has a higher decomposition temperature than hemicellulose. The degrading peak at 1102 cm^{-1} corresponds to C–O vibrations in cellulose. Additionally, the change in the peaks at approximately 1155 cm^{-1} suggests its mild degradation. The highest peak, which for all samples has a maximum of approximately 1030 cm^{-1} and merges with the signal at 1051 cm^{-1} , is from the stretching vibration of the C–O bond in aliphatic ether and alcohol, respectively [49]. The results confirm that USF has some organic origin. The decrease in intensity of the signal for the hydrochars can be associated with the fact that some of the bonds were broken during the hydrothermal process.

3.3. Scanning Electron Microscopy with Energy Dispersive X-ray Spectroscopy

In the images received via scanning electron microscopy (Figure 8) a fibrous structure of untreated under-sieve fraction of municipal mixed waste can be seen. The hydrothermal carbonization process significantly alters the structure and morphology of the material. In Figure 8b there are still many elongated particles visible, however they are much shorter than those presented for untreated USF in Figure 8a. In the following Figure 8c,d, samples after a longer residence time are depicted. The open, circular pores in Figure 8c prove that some of the volatile matter is released during the HTC process, which may cause higher surface degradation but also a higher specific surface area. It can be seen that with an increase in the residence time of the process, the quantity of fine particles also increases. This can influence not only the combustion behavior of hydrochar but also its dewaterability. EDS analysis (Table 4) distinguished mainly carbon and oxygen, but calcium, silicon, and sulphur can also be observed, among other elements. This provides valuable information concerning potential challenges, such as slagging and fouling or corrosion, which may occur in a scaled-up process [50,51].

Table 3. Indicator bands, their vibrations, and corresponding functional groups.

Wavenumber (cm^{-1})	Vibration	Functional Group or Component
3600–3100	O–H stretch	hydroxyl or carboxyl group
2930–2860	C–H stretch	aliphatic methylene group
1740	C=O	alkali esters in hemicellulose
~1515	C=O	lignin
~1455	C–H	lignin
1102	C–O	cellulose
1050	C–O stretch	alcohol
1030	C–O stretch	aliphatic ether

Table 4. Results of EDS analysis (ZAF method), wt%.

	C K	N K	O K	F K	Cu L	Na K	Mg K	Al K	Si K	P K	S K	Cl K	K K	Ca K	Ti K	Fe K
USF	66.31	1.24	28.87	0.15	0.19	0.33	0.17	0.33	0.74	0.00	0.17	0.20	0.09	0.86	0.08	0.27
220_1 h	66.95	1.45	28.29	0.08	0.08	0.28	0.21	0.38	1.21	0.06	0.16	0.05	0.05	0.52	0.14	0.10
220_4 h	75.21	0.99	20.94	0.08	0.13	0.19	0.16	0.32	1.09	0.02	0.17	0.03	0.00	0.39	0.08	0.20
220_8 h	75.37	1.20	19.83	0.08	0.20	0.16	0.16	0.40	1.21	0.06	0.27	0.08	0.10	0.47	0.16	0.25

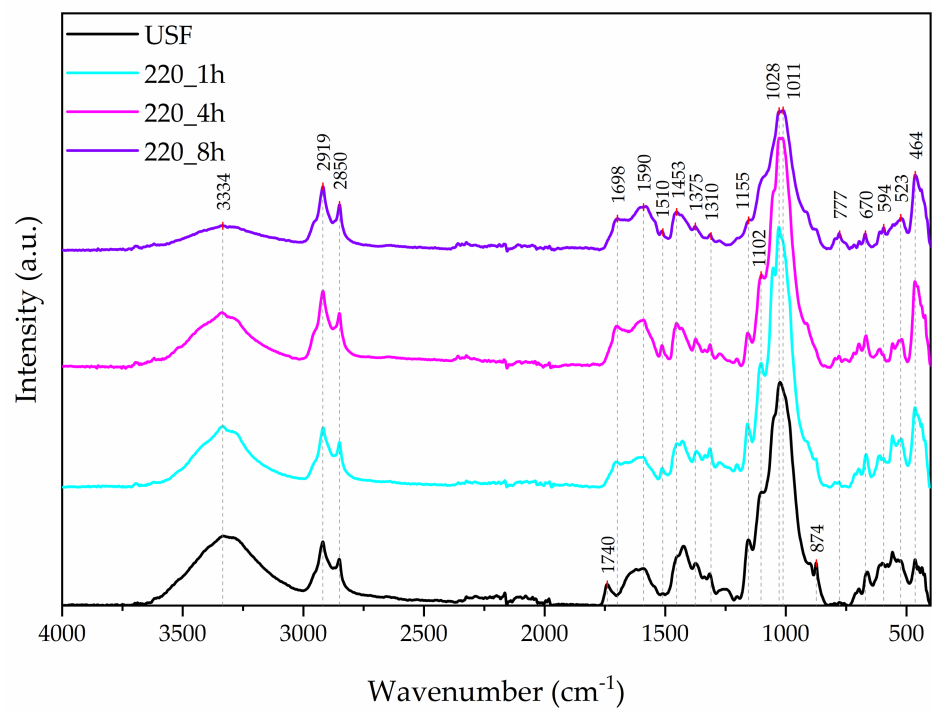
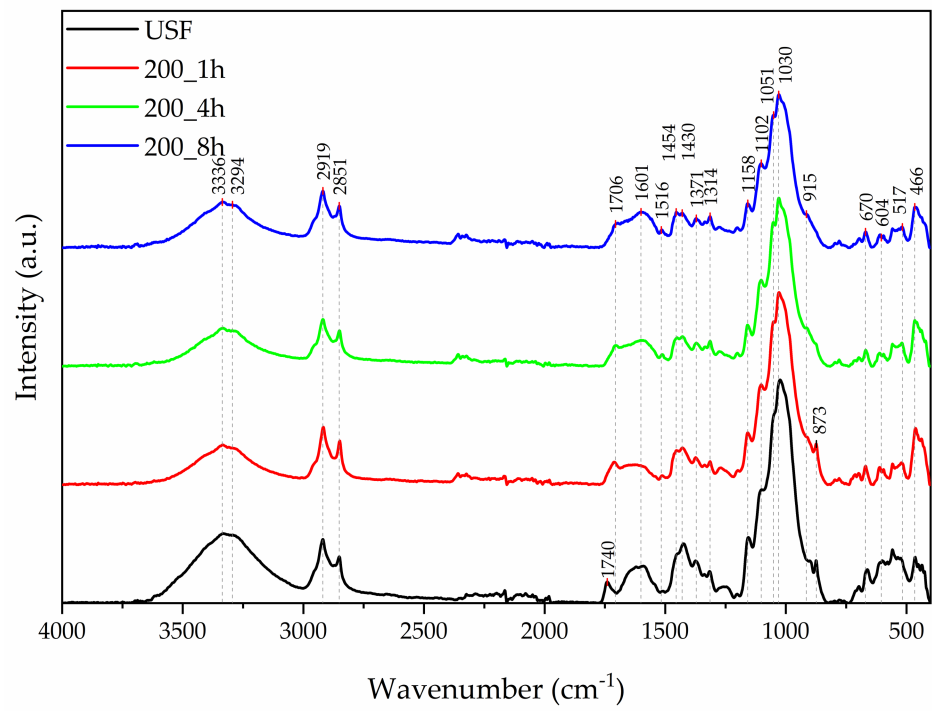


Figure 7. FTIR spectra of the USF and hydrochars.

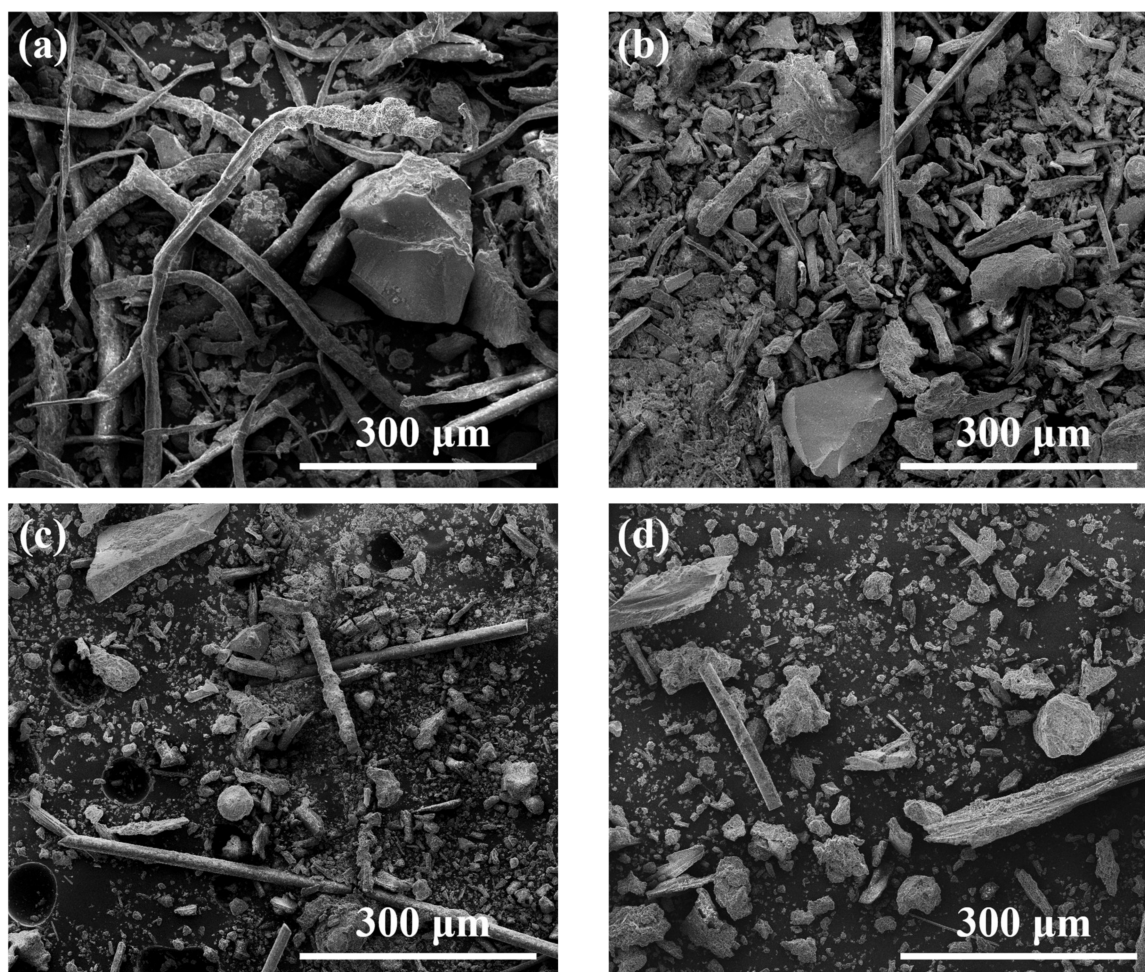


Figure 8. SEM images of (a) USF and hydrochars produced at 220 °C for (b) 1 h; (c) 4 h; (d) 8 h.

4. Conclusions

Hydrothermal carbonization of the under-sieve fraction of municipal mixed solid waste was performed. Conducted analyses proved that the hydrothermal process altered the structure and other physical and chemical properties of USF. The most promising results were found for hydrochar produced at 220 °C for 1 h leading to a better combustion performance and providing a more stable and a less violent flame. This was confirmed by combustibility indices $S = 12.4 \times 10^{-8} \% \cdot \text{min}^{-2} \cdot \text{°C}^{-3}$, $H_f = 1174.9 \text{ °C}$, and $D_i = 0.0075 \% \cdot \text{min}^{-3}$, which in comparison to USF decreased by 44%, increased by 33%, and decreased by 29%, respectively. The correlation between the process parameters and the analysis results was proved. The changed morphology after the hydrothermal process results in easier grinding, handling, and dewatering of hydrochars. Further, detailed analysis may aid understanding in how process parameters influence the specific properties of hydrochars. Nevertheless, an improvement in the performance of mixed solid waste as a fuel by transforming it into hydrochar was confirmed.

Author Contributions: Conceptualization, L.L. and M.W.; methodology, L.L., M.W. and A.M.; validation, M.Ś., K.C. and A.M.; investigation, M.Ś., K.C. and A.M.; resources, L.L. and M.W.; data curation, M.Ś., K.C. and A.M.; writing—original draft preparation, M.Ś. and M.W.; writing—review and editing, L.L. and M.W.; visualization, M.Ś.; supervision, L.L. and M.W. All authors have read and agreed to the published version of the manuscript.

Funding: The research was financed by the Ministry of Science and Higher Education [AGH UST grant no. 16.16.110.663].

Institutional Review Board Statement: Not applicable.

Informed Consent Statement: Not applicable.

Data Availability Statement: The data presented in this study are available on request from the corresponding author.

Acknowledgments: The authors would like to thank the proprietor of the experimental apparatus EKOPROD Ltd. in Bytom.

Conflicts of Interest: The authors declare no conflict of interest. The funders had no role in the design of the study; in the collection, analyses, or interpretation of data; in the writing of the manuscript; or in the decision to publish the results.

References

1. Wilk, M.; Śliz, M.; Gajek, M. The Effects of Hydrothermal Carbonization Operating Parameters on High-Value Hydrochar Derived from Beet Pulp. *Renew. Energy* **2021**, *177*, 216–228. [[CrossRef](#)]
2. Saqib, N.U.; Sharma, H.B.; Baroutian, S.; Dubey, B.; Sarmah, A.K. Valorisation of Food Waste via Hydrothermal Carbonisation and Techno-Economic Feasibility Assessment. *Sci. Total Environ.* **2019**, *690*, 261–276. [[CrossRef](#)]
3. Gupta, D.; Mahajani, S.M.; Garg, A. Effect of Hydrothermal Carbonization as Pretreatment on Energy Recovery from Food and Paper Wastes. *Bioresour. Technol.* **2019**, *285*, 121329. [[CrossRef](#)]
4. Wilk, M.; Śliz, M.; Lubieniecki, B. Hydrothermal Co-Carbonization of Sewage Sludge and Fuel Additives: Combustion Performance of Hydrochar. *Renew. Energy* **2021**, *178*, 1046–1056. [[CrossRef](#)]
5. Lin, Y.; Ma, X.; Peng, X.; Yu, Z. Hydrothermal Carbonization of Typical Components of Municipal Solid Waste for Deriving Hydrochars and Their Combustion Behavior. *Bioresour. Technol.* **2017**, *243*, 539–547. [[CrossRef](#)]
6. Triyono, B.; Prawisudha, P.; Aziz, M.; Mardiyati; Pasek, A.D.; Yoshikawa, K. Utilization of Mixed Organic-Plastic Municipal Solid Waste as Renewable Solid Fuel Employing Wet Torrefaction. *Waste Manag.* **2019**, *95*, 1–9. [[CrossRef](#)]
7. Czerwińska, K.; Śliz, M.; Wilk, M. Hydrothermal Carbonization Process: Fundamentals, Main Parameter Characteristics and Possible Applications Including an Effective Method of SARS-CoV-2 Mitigation in Sewage Sludge. A Review. *Renew. Sustain. Energy Rev.* **2022**, *154*, 111873. [[CrossRef](#)]
8. Merzari, F.; Goldfarb, J.; Andreottola, G.; Mimmo, T.; Volpe, M.; Fiori, L. Hydrothermal Carbonization as a Strategy for Sewage Sludge Management: Influence of Process Withdrawal Point on Hydrochar Properties. *Energies* **2020**, *13*, 2890. [[CrossRef](#)]
9. Wilk, M. A Novel Method of Sewage Sludge Pre-Treatment—HTC. *E3S Web Conf.* **2016**, *10*, 00103. [[CrossRef](#)]
10. Jakubus, M.; Stejskal, B. Municipal Solid Waste Management Systems in Poland and the Czech Republic. A Comparative Study. *Environ. Prot. Eng.* **2020**, *46*, 61–78. [[CrossRef](#)]
11. Lin, Y.; Ma, X.; Peng, X.; Yu, Z.; Fang, S.; Lin, Y.; Fan, Y. Combustion, Pyrolysis and Char CO₂-Gasification Characteristics of Hydrothermal Carbonization Solid Fuel from Municipal Solid Wastes. *Fuel* **2016**, *181*, 905–915. [[CrossRef](#)]
12. Magdziarz, A.; Mlonka-Mędrala, A.; Sieradzka, M.; Aragon-Briceño, C.; Pożarlik, A.; Bramer, E.A.; Brem, G.; Niedzwiecki, Ł.; Pawlak-Kruczek, H. Multiphase Analysis of Hydrochars Obtained by Anaerobic Digestion of Municipal Solid Waste Organic Fraction. *Renew. Energy* **2021**, *175*, 108–118. [[CrossRef](#)]
13. Heidari, M.; Dutta, A.; Acharya, B.; Mahmud, S. A Review of the Current Knowledge and Challenges of Hydrothermal Carbonization for Biomass Conversion. *J. Energy Inst.* **2019**, *92*, 1779–1799. [[CrossRef](#)]
14. Lühmann, T.; Wirth, B. Sewage Sludge Valorization via Hydrothermal Carbonization: Optimizing Dewaterability and Phosphorus Release. *Energies* **2020**, *13*, 4417. [[CrossRef](#)]
15. Santos, M.M.; Diez, M.A.; Suárez, M.; Centeno, T.A. Innovative Particleboard Material from the Organic Fraction of Municipal Solid Waste. *J. Build. Eng.* **2021**, *44*, 103375. [[CrossRef](#)]
16. Ischia, G.; Fiori, L.; Gao, L.; Goldfarb, J.L. Valorizing Municipal Solid Waste via Integrating Hydrothermal Carbonization and Downstream Extraction for Biofuel Production. *J. Clean. Prod.* **2021**, *289*, 125781. [[CrossRef](#)]
17. Aragon-Briceño, C.; Pożarlik, A.; Bramer, E.; Brem, G.; Wang, S.; Wen, Y.; Yang, W.; Pawlak-Kruczek, H.; Niedzwiecki, Ł.; Urbanowska, A.; et al. Integration of Hydrothermal Carbonization Treatment for Water and Energy Recovery from Organic Fraction of Municipal Solid Waste Digestate. *Renew. Energy* **2022**, *184*, 577–591. [[CrossRef](#)]
18. Espro, C.; Satira, A.; Mauriello, F.; Anajafi, Z.; Moulalee, K.; Iannazzo, D.; Neri, G. Orange Peels-Derived Hydrochar for Chemical Sensing Applications. *Sens. Actuators B Chem.* **2021**, *341*, 130016. [[CrossRef](#)]
19. Roman, F.F.; Diaz De Tuesta, J.L.; Praça, P.; Silva, A.M.T.; Faria, J.L.; Gomes, H.T. Hydrochars from Compost Derived from Municipal Solid Waste: Production Process Optimization and Catalytic Applications. *J. Environ. Chem. Eng.* **2021**, *9*, 104888. [[CrossRef](#)]
20. Lin, Y.; Ge, Y.; Xiao, H.; He, Q.; Wang, W.; Chen, B. Investigation of Hydrothermal Co-Carbonization of Waste Textile with Waste Wood, Waste Paper and Waste Food from Typical Municipal Solid Wastes. *Energy* **2020**, *210*, 118606. [[CrossRef](#)]
21. Venna, S.; Sharma, H.B.; Reddy, P.H.P.; Chowdhury, S.; Dubey, B.K. Landfill Leachate as an Alternative Moisture Source for Hydrothermal Carbonization of Municipal Solid Wastes to Solid Biofuels. *Bioresour. Technol.* **2021**, *320*, 124410. [[CrossRef](#)] [[PubMed](#)]

22. Wang, T.; Zhai, Y.; Zhu, Y.; Gan, X.; Zheng, L.; Peng, C.; Wang, B.; Li, C.; Zeng, G. Evaluation of the Clean Characteristics and Combustion Behavior of Hydrochar Derived from Food Waste towards Solid Biofuel Production. *Bioresour. Technol.* **2018**, *266*, 275–283. [[CrossRef](#)] [[PubMed](#)]
23. Akarsu, K.; Duman, G.; Yilmazer, A.; Keskin, T.; Azbar, N.; Yanik, J. Sustainable Valorization of Food Wastes into Solid Fuel by Hydrothermal Carbonization. *Bioresour. Technol.* **2019**, *292*, 121959. [[CrossRef](#)] [[PubMed](#)]
24. Saqib, N.U.; Baroutian, S.; Sarmah, A.K. Physicochemical, Structural and Combustion Characterization of Food Waste Hydrochar Obtained by Hydrothermal Carbonization. *Bioresour. Technol.* **2018**, *266*, 357–363. [[CrossRef](#)]
25. Nguyen, D.; Zhao, W.; Mäkelä, M.; Alwahabi, Z.T.; Kwong, C.W. Effect of Hydrothermal Carbonisation Temperature on the Ignition Properties of Grape Marc Hydrochar Fuels. *Fuel* **2022**, *313*, 122668. [[CrossRef](#)]
26. Sharma, H.B.; Sarmah, A.K.; Dubey, B. Hydrothermal Carbonization of Renewable Waste Biomass for Solid Biofuel Production: A Discussion on Process Mechanism, the Influence of Process Parameters, Environmental Performance and Fuel Properties of Hydrochar. *Renew. Sustain. Energy Rev.* **2020**, *123*, 109761. [[CrossRef](#)]
27. Yang, Y.; Wang, J.; Chong, K.; Bridgwater, A.V. A Techno-Economic Analysis of Energy Recovery from Organic Fraction of Municipal Solid Waste (MSW) by an Integrated Intermediate Pyrolysis and Combined Heat and Power (CHP) Plant. *Energy Convers. Manag.* **2018**, *174*, 406–416. [[CrossRef](#)]
28. Zhou, H.; Long, Y.; Meng, A.; Li, Q.; Zhang, Y. Classification of Municipal Solid Waste Components for Thermal Conversion in Waste-to-Energy Research. *Fuel* **2015**, *145*, 151–157. [[CrossRef](#)]
29. Wang, T.; Zhai, Y.; Zhu, Y.; Li, C.; Zeng, G. A Review of the Hydrothermal Carbonization of Biomass Waste for Hydrochar Formation: Process Conditions, Fundamentals, and Physicochemical Properties. *Renew. Sustain. Energy Rev.* **2018**, *90*, 223–247. [[CrossRef](#)]
30. Basso, D.; Patuzzi, F.; Castello, D.; Baratieri, M.; Rada, E.C.; Weiss-Hortala, E.; Fiori, L. Agro-Industrial Waste to Solid Biofuel through Hydrothermal Carbonization. *Waste Manag.* **2016**, *47*, 114–121. [[CrossRef](#)]
31. Berge, N.D.; Ro, K.S.; Mao, J.; Flora, J.R.V.; Chappell, M.A.; Bae, S. Hydrothermal Carbonization of Municipal Waste Streams. *Environ. Sci. Technol.* **2011**, *45*, 5696–5703. [[CrossRef](#)] [[PubMed](#)]
32. Śliz, M.; Tuci, F.; Czerwińska, K.; Fabrizi, S.; Lombardi, L.; Wilk, M. Hydrothermal Carbonization of the Wet Fraction from Mixed Municipal Solid Waste: Hydrochar Characteristics and Energy Balance. *Waste Manag.* **2022**, *151*, 39–48. [[CrossRef](#)] [[PubMed](#)]
33. Parshetti, G.K.; Kent Hoekman, S.; Balasubramanian, R. Chemical, Structural and Combustion Characteristics of Carbonaceous Products Obtained by Hydrothermal Carbonization of Palm Empty Fruit Bunches. *Bioresour. Technol.* **2013**, *135*, 683–689. [[CrossRef](#)] [[PubMed](#)]
34. Lu, J.J.; Chen, W.H. Investigation on the Ignition and Burnout Temperatures of Bamboo and Sugarcane Bagasse by Thermogravimetric Analysis. *Appl. Energy* **2015**, *160*, 49–57. [[CrossRef](#)]
35. Sieradzka, M.; Gao, N.; Quan, C.; Mlonka-Mędrala, A.; Magdziarz, A. Biomass Thermochemical Conversion via Pyrolysis with Integrated CO₂ Capture. *Energies* **2020**, *13*, 1050. [[CrossRef](#)]
36. Mureddu, M.; Dessì, F.; Orsini, A.; Ferrara, F.; Pettinau, A. Air- and Oxygen-Blown Characterization of Coal and Biomass by Thermogravimetric Analysis. *Fuel* **2018**, *212*, 626–637. [[CrossRef](#)]
37. Wang, L.; Chang, Y.; Zhang, X.; Yang, F.; Li, Y.; Yang, X.; Dong, S. Hydrothermal Co-Carbonization of Sewage Sludge and High Concentration Phenolic Wastewater for Production of Solid Biofuel with Increased Calorific Value. *J. Clean. Prod.* **2020**, *255*, 120317. [[CrossRef](#)]
38. Dolgen, D.; Sarptas, H.; Alpaslan, N.; Kucukgul, O. Energy Potential of Municipal Solid Wastes. *Energy Sources* **2005**, *27*, 1483–1492. [[CrossRef](#)]
39. Komilis, D.; Kissas, K.; Symeonidis, A. Effect of Organic Matter and Moisture on the Calorific Value of Solid Wastes: An Update of the Tanner Diagram. *Waste Manag.* **2014**, *34*, 249–255. [[CrossRef](#)]
40. Nizamuddin, S.; Baloch, H.A.; Griffin, G.J.; Mubarak, N.M.; Bhutto, A.W.; Abro, R.; Mazari, S.A.; Ali, B.S. An Overview of Effect of Process Parameters on Hydrothermal Carbonization of Biomass. *Renew. Sustain. Energy Rev.* **2017**, *73*, 1289–1299. [[CrossRef](#)]
41. Wang, J.; Liu, H.; Deng, H.; Jin, M.; Xiao, H.; Yao, H. Deep Dewatering of Sewage Sludge and Simultaneous Preparation of Derived Fuel via Carbonaceous Skeleton-Aided Thermal Hydrolysis. *Chem. Eng. J.* **2020**, *402*, 126255. [[CrossRef](#)]
42. Zheng, C.; Ma, X.; Yao, Z.; Chen, X. The Properties and Combustion Behaviors of Hydrochars Derived from Co-Hydrothermal Carbonization of Sewage Sludge and Food Waste. *Bioresour. Technol.* **2019**, *285*, 121347. [[CrossRef](#)] [[PubMed](#)]
43. Pawlak-Kruczek, H.; Niedzwiecki, L.; Sieradzka, M.; Mlonka-Mędrala, A.; Baranowski, M.; Serafin-Tkaczuk, M.; Magdziarz, A. Hydrothermal Carbonization of Agricultural and Municipal Solid Waste Digestates—Structure and Energetic Properties of the Solid Products. *Fuel* **2020**, *275*, 117837. [[CrossRef](#)]
44. Lin, Y.; Ma, X.; Ning, X.; Yu, Z. TGA-FTIR Analysis of Co-Combustion Characteristics of Paper Sludge and Oil-Palm Solid Wastes. *Energy Convers. Manag.* **2015**, *89*, 727–734. [[CrossRef](#)]
45. Arellano, O.; Flores, M.; Guerra, J.; Hidalgo, A.; Rojas, D.; Strubinger, A. Hydrothermal Carbonization of Corncob and Characterization of the Obtained Hydrochar. *Chem. Eng. Trans.* **2016**, *50*, 235–240. [[CrossRef](#)]
46. He, C.; Zhao, J.; Yang, Y.; Wang, J.Y. Multiscale Characteristics Dynamics of Hydrochar from Hydrothermal Conversion of Sewage Sludge under Sub- and near-Critical Water. *Bioresour. Technol.* **2016**, *211*, 486–493. [[CrossRef](#)]
47. Lang, Q.; Guo, Y.; Zheng, Q.; Liu, Z.; Gai, C. Co-Hydrothermal Carbonization of Lignocellulosic Biomass and Swine Manure: Hydrochar Properties and Heavy Metal Transformation Behavior. *Bioresour. Technol.* **2018**, *266*, 242–248. [[CrossRef](#)]

48. Nizamuddin, S.; Jaya Kumar, N.S.; Sahu, J.N.; Ganesan, P.; Mubarak, N.M.; Mazari, S.A. Synthesis and Characterization of Hydrochars Produced by Hydrothermal Carbonization of Oil Palm Shell. *Can. J. Chem. Eng.* **2015**, *93*, 1916–1921. [[CrossRef](#)]
49. Petrović, J.; Perišić, N.; Maksimović, J.D.; Maksimović, V.; Kragović, M.; Stojanović, M.; Laušević, M.; Mihajlović, M. Hydrothermal Conversion of Grape Pomace: Detailed Characterization of Obtained Hydrochar and Liquid Phase. *J. Anal. Appl. Pyrolysis* **2016**, *118*, 267–277. [[CrossRef](#)]
50. Ghosh, D.; Mitra, S.K. High Temperature Corrosion Problem of Boiler Components in Presence of Sulfur and Alkali Based Fuels. *High Temp. Mater. Processes* **2011**, *30*, 81–85. [[CrossRef](#)]
51. Kou, X.; Jin, J.; Wang, Y.; Li, Y.; Hou, F. Understanding the Effect of Calcium Containing Compounds on Ash Deposition during Boiler Operation: Experiment Study and Dynamics Calculation. *Environ. Sci. Pollut. Res.* **2022**, *1*, 1–14. [[CrossRef](#)] [[PubMed](#)]